Variable Inclination Continuous Transverse Stub Array-Based Beam Steering Antenna System for Vehicle-to-Satellite Communication

S. Y. LIU [1,2], C. F. ZHOU [3] (Member, IEEE), J. LIU[2], J. H. FU [1],
Q. WU[1] (Senior Member, IEEE), AND X. M. DING [1]

[1]Department of Microwave Engineering, Harbin Institute of Technology, Harbin 150001, China

[2]Department of Antenna Technology, Beijing Institute of Remote Sensing Equipment, Beijing 100854, China

[3]School of Information and Communication Engineering, Dalian University of Technology, Dalian 116024, China

CORRESPONDING AUTHORS: C. F. ZHOU and X. M. DING (e-mail: cfzhou@dlut.edu.cn; xuminding@hit.edu.cn)

ABSTRACT A Ku-band variable inclination continuous transverse stub (VICTS) antenna system for vehicle-to-satellite communication is designed with high gain and low sidelobe level (SLL). Taylor distribution is used to determine the radiation power for each slot by extracting the admittance of each slot to achieve a low SLL. The antenna system contains the VICTS antenna and the servo control system. The servo control system is used to rotate the feeding and radiating plates of the VICTS antenna to realize beam steering. The feeding plate is placed underneath the radiating plate for a compact size. For verifying the concept, the antenna system is prototyped and measured. The measured results show that within 13.75-14.5 GHz, the voltage standing wave ratio (VSWR) is below 1.4. A large beam scanning range of $7° \sim 64°$ or $-7° \sim -64°$ in elevation and $360°$ in azimuth is achieved, with a maximum gain of 32.1 dBi. For all the scanning angles, the SLLs maintain lower than -16.5 dB.

INDEX TERMS Beam scanning, variable inclination continuous transverse stub (VICTS), high gain.

I. INTRODUCTION

REAL-TIME communication and high-speed recognition techniques are highly demanded for high-speed wireless communication systems on the move, such as the vehicle radar system and Satellite Communications (SatCom) on the move [1]. In the scenario where the 5G base station cannot maintain the available communication, the vehicle needs to communicate with the low-earth-orbit (LEO) satellite for high-quality data transmitting and receiving [2]. The fusion of the 5G core network and LEO satellite communication network can be a good solution for cost and communication coverage. As a result, beam steering corresponds to different locations when the vehicle moves fast, as shown in Fig. 1. To further facilitate communication in the area where the base station cannot cover, a beam-steering antenna system [3] is required in both the vehicle and satellite terminals.

In the applications of radar and SatCom systems, the parabolic reflector antenna is widely employed due to the high beam-pointing precision [4], but its volume is bulky and it suffers great wind resistance when the platform is moving at a high speed. To satisfy the aesthetic and aerodynamic requirements, the antenna should be low profile, compact, low weight, low cost, and mechanically robust [5]. Particularly, long-distance communication requires the antenna to have a high gain with a narrow beamwidth to compensate for the propagation loss. In this context, it is better for the antennas at both terminals (base station and user terminals) to own the capability of beam steering to find each other. There are several methods to realize the beam scanning function, such as mechanical and electronic scanning. Mechanical scanning antenna systems make use of the three-dimensional servo platform to control
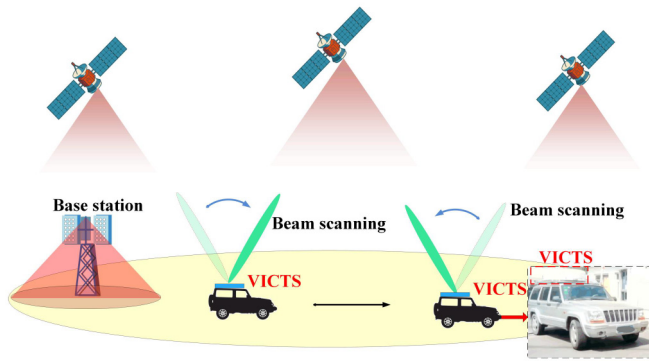
FIGURE 1. Vehicle-to-satellite communication scenario.

the beam direction of an antenna [6], whose radiation pattern is usually fixed without the rotary platform. However, the profile of this system is very high, which cannot satisfy the dynamic requirement of the high-speed vehicle. In [7], rotary metasurface is used to achieve beam scanning in azimuth above a patch antenna, but the main-beam direction can only be fixed at an angle of 32° from the broadside in elevation. The phased array antenna is a more flexible method, but the phase shifter module of the phased array is complex and expensive [8]. As a result, researchers have investigated many works on the pattern reconfigurable antenna with a low profile and low cost [9], [10], [11], [12]. However, the beam could not be steered continuously since the radiation pattern could only be switched among several states.

Due to the low profile and mechanical robustness, a continuous transverse stub (CTS) array antenna can be a good candidate for beam scanning in the high-speed communication system for LEO satellites. As a new kind of leaky-wave antenna, the CTS array was first proposed by Milroy in the 1990s [13], [14], and the electromagnetic energy is radiated from the slots between the transverse stubs. The CTS array antenna can be fed in a parallel [5], [15], [16], [17] or series [18], [19], [20], [21], [22], [23] way, with the CTS in the upper plate and the feeding structure in the lower layer. The feeding techniques, such as the coplanar waveguide (CPW) [20], coaxial cable [22], and the parallel plate waveguide (PPW) [23] structure are often adopted to feed the CTS array. Through the asynchronous or synchronous rotation between these two plates, beam steering can be achieved [18], [23]. In [18], a maximum gain of 29.3 dBi is achieved, and its sidelobe level (SLL) is below −14 dB. The antenna in [23] has a maximum gain of 29.2 dBi, but the SLL is relatively high at −9 dB. To enhance the anti-interference ability of the communication system, achieving a low side lobe is quite challenging and necessary.

In this paper, a variable inclination continuous transverse stub (VICTS) beam scanning antenna system operating in Ku-band (13.75-14.5 GHz) for SatCom on the move is presented. The VICTS antenna is designed with two plates, i.e., the VICTS slot array is developed as the radiating part in the upper layer, and the slow-wave structure and the PPW are used as the feeding part in the lower layer.

The admittance of the slot by varying the slot width is extracted, then, the Taylor distribution is used to determine the radiation power for each slot to achieve a low sidelobe level. To avoid energy leakage due to the isolation air gap, a high-impedance choke groove behind the coupling slot is employed to reflect the EM wave to the slow-wave structure. Besides the VICTS antenna, the servo control module is considered in our antenna system to control the rotation of the feeding of the radiating parts. Compared with other VICTS beam steering antennas [18], [23], a higher gain of 32.1 dBi and a lower SLL of −16.5 dB are achieved. Measured results show that the proposed antenna can achieve a continuous wide beam scanning range of 7° ∼ 64° or −7° ∼ −64° in elevation and 360° in azimuth. For all the scanning angles, the gains range between 26.4 and 32.1 dBi, and the SLLs are lower than −16.5 dB. Due to the performances of high mobility, wide beam scanning range, high gain, and low SLL, the proposed VICTS antenna system can be applied in the mobile ground terminals for LEO satellite communication.

II. ANTENNA DESIGN
A. ANTENNA CONFIGURATION
The proposed CTS array antenna is shown in Fig. 2, consisting of three-layer blocks: the radiation structure in the upper layer M1, the feeding structure in the middle layer M2, and the lower layer M3. The radiation structure contains a periodic array of 27 radiation slots cut in the metal plate in the top layer M1. The feeding part is composed of the slow-wave structure in layer M2 and the PPW in layer M3. The CTS array antenna has a total volume of $\pi \times R \times R \times H$, ($R = 250$ mm, $H = 27$ mm, $\pi \times 11.9 \times 11.9 \times 1.28\ \lambda^3$, λ is the space wavelength at 14.25 GHz).

The PPW in layer M3 contains a standard input waveguide (WJB-140) and a 1-to-16 waveguide power divider. Then, a turnover structure acting as a coupling slot at the ends of PPW is used to connect the slow-wave structure. As the turnover structure locates in both M2 and M3 layers, we define it as "turnover structure". The energy is transmitted through the coupling slot to the slow-wave structure, then radiated to space. Here, the PPW is placed under the CTS array and the slow-wave structure to achieve a compact size, as shown in Fig. 2(b).

To achieve beam scanning, the rotation between the radiating and the feeding plates is needed. Hence, an isolation air layer with a height of 1.5 mm is required to maintain the independent rotation, as shown in Fig. 2. Due to the air layer, the electromagnetic (EM) wave will be leaked out. To solve this problem, we have added a high-impedance choke groove behind the coupling slot, which can reflect the EM wave to the slow-wave structure. In addition, the absorption material is placed around the slow-wave structure in layer M2 to further minimize the energy leakage.

B. CST RADIATION SLOTS
The radiation part owns 27 narrow slots, and the radiation principle is similar to that of the leaky-wave slot array
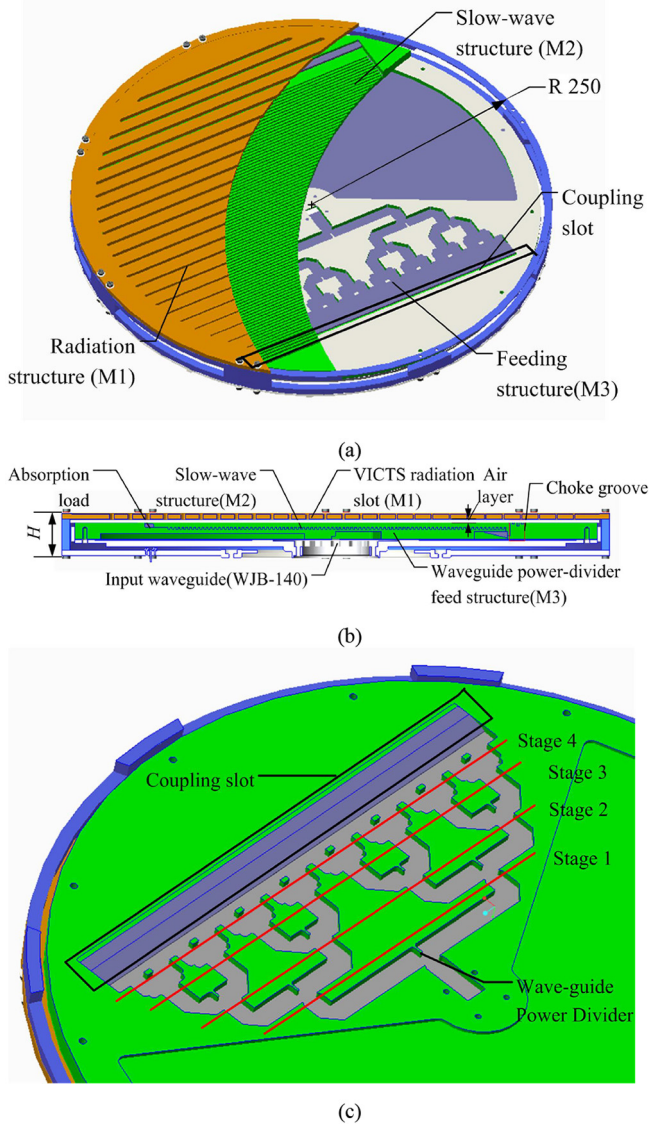
FIGURE 2. (a) 3D view (b) side view, and (c) back view of the CTS array antenna.

antenna [24]. The widths of the radiation slots are varied to control the power coupled from the slow-wave structure, which determines the radiation of the proposed antenna. The slots can be designed according to [25],

$$g = qr^{-1/n} - 1 \quad (1)$$

where g is the admittance of a slot, q is the attenuation coefficient of the waveguide, n is the number of the slots, and r indicates the ratio of the power absorbed by end load to the input electromagnetic power expressed as:

$$r = \frac{|S_{21}|^2}{1 - |S_{11}|^2} \quad (2)$$

If the height of each slot is fixed at 5 mm, we can get the admittance of the slot by varying the slot width as shown in Fig. 3. It can be seen that the admittance increases with the increase of the slot width. To achieve a low sidelobe of the

TABLE 1. Widths and admittances of slot based on Taylor distribution.

No.	Admittance (S)	width (mm)	No.	Admittance (S)	width (mm)
1	0.0124	1.4	15	0.2259	3.35
2	0.0124	1.4	16	0.2538	3.5
3	0.0131	1.4	17	0.2778	3.55
4	0.0148	1.4	18	0.2881	3.6
5	0.0185	1.4	19	0.2806	3.6
6	0.0188	1.4	20	0.2714	3.55
7	0.0212	1.5	21	0.2910	3.65
8	0.0277	1.65	22	0.3714	3.9
9	0.0410	1.9	23	0.5909	4.6
10	0.0616	2.2	24	0.5909	4.6
11	0.0877	2.5	25	0.5909	4.6
12	0.1177	2.7	26	0.5909	4.6
13	0.1533	3	27	0.5909	4.6
14	0.1982	3.2			

CTS array antenna, we use the Taylor distribution [26] of the radiation power for each slot when the relative rotation angle between the feeding and radiating parts is 0°. According to

$$g_i = \frac{P_i}{P_i'} = 1 + 2 \sum_{i}^{n-1} s(i, A, n) \cos\left(\frac{2i\pi}{L} z_i\right) \quad (3)$$

$$s(i, A, n) = \frac{[(n-1)!]^2}{(n-1+i)!(n-1-i)!}$$
$$\times \prod_{i=1}^{n-1} \left\{ 1 - \frac{i^2}{\sigma^2 [A^2 + (n-0.5)]^2} \right\} \quad (4)$$

$$A = \arccos\left(10^{SLR/20}\right)/\pi \quad (5)$$

$$\sigma = n/\sqrt{A^2 + (n-0.5)^2} \quad (6)$$

where P_i is the radiated power of the i-th slot, P_i' is the remained power towards the load, g_i is the admittance of the i-th slot, SLR is the desired sidelobe level as -25 dB, L is the total length of all the slots, and z_i is the i-th slot location distance. The elementary radiating unit cell is exhibited in Fig. 3. Based on the model in Fig. 3, S11 and S21 are obtained from the HFSS simulation. The admittance g_i is calculated from equations (1) and (2). Then, we can get the admittance of each slot with different widths, and the relation between the admittance and the width is shown in Fig. 4. By setting the sidelobe level as -25 dB, the admittance of each slot can be obtained based on the formulas of Taylor distribution (3)-(6). According to the admittance distribution by Taylor distribution, the widths of the slots are chosen in Table 1. Table 1 shows the related value of the width and the admittance.

C. FEEDING STRUCTURE
The feeding structure contains two parts, i.e., the slow-wave structure in layer M2 and the feeding waveguide in layer M3. A standard input waveguide (WJB-140) is followed by a 1-to-16 waveguide power divider, then transit
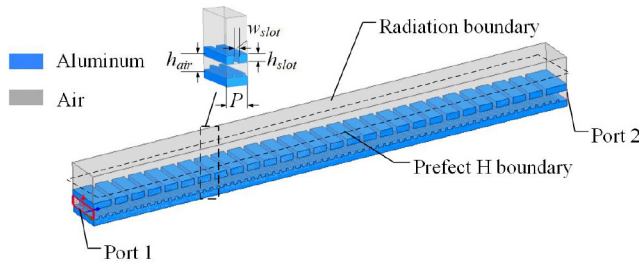
FIGURE 3. Unit cell structure, (p = 17mm, h_{air} = 8mm, h_{slot} = 5mm).

FIGURE 4. Admittances of slots with different widths.

FIGURE 5. Side view of the radiation slots, slow-wave structure, and turnover structure.

FIGURE 6. Structure of the last stage power divider.

FIGURE 7. E-field distribution with and without step adjuster 2.

to the waveguide. A turnover structure in Fig. 5, acting as a coupling slot, is used at the end of the feeding waveguide to connect the slow-wave structure. The dimension of step adjuster 1 can be used to achieve good matching. The function of the slow-wave structure is to shorten the waveguide wavelength in the air-filled PPW to inhibit the sidelobe [19]. The waveguide wavelength depends on the height, width, and adjacent distance of the unit of the slow-wave structure. Meanwhile, the dimension of the unit should consider the fabrication tolerance. In this design, h = 2 mm, w = 2 mm, and d = 3.85 mm are selected.

In layer M3, a 1-to-16 waveguide power divider is first designed with 4 stages, as shown in Fig. 2. The energy is input from the 1-to-16 waveguide power divider, then transmits through the coupling slot and slow-wave structure to excite the CTS array slots. The remaining energy is absorbed by the absorption material around the slow-wave structure. In addition, step adjuster 2, as shown in Fig. 6, is added to generate the quasi-TEM wave in the waveguide. To show the function of the step adjuster, the E-fields of the feeding network with and without the step adjuster are shown in Fig. 7. It can be seen that the step adjuster helps to generate the quasi-TEM wave in the PPW, which is in-phase along the transverse direction to excite the radiation slots effectively.

For easy rotating the layers M2 and M3, a thin slot layer is added between the radiation and feeding parts shown in Fig. 5, which may cause energy leakage, resulting in low
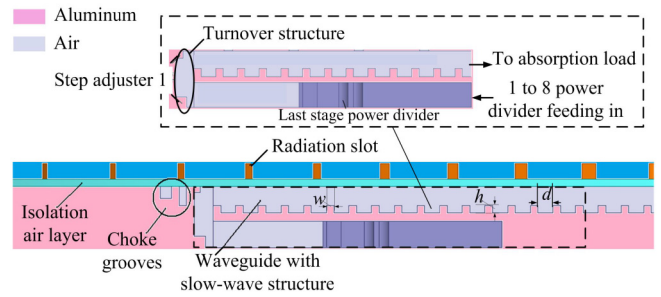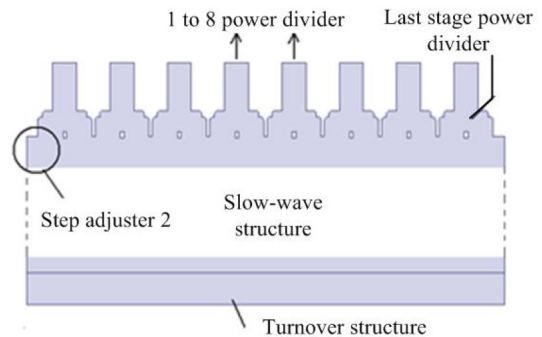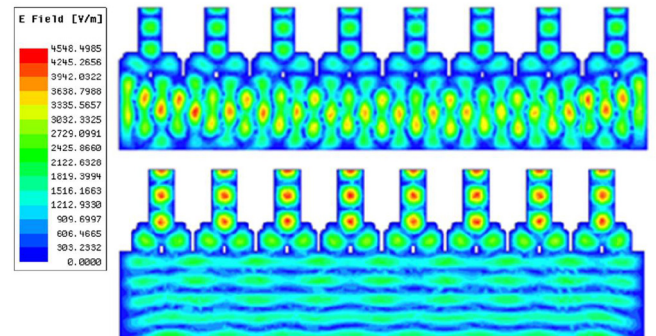
efficiency. Thus, avoiding energy leakage is necessary. The high-impedance choke groove structure in Fig. 5 is loaded behind the feeding network, which is used for reflecting the leaked EM wave to the slow-wave structure. We have compared the E-fields of the proposed antenna with and without the high-impedance choke groove structure in Fig. 8, indicating that the choke groove structure can effectively inhibit energy leakage. In layer M3, the EM wave is travelling from the right to the left, while the EM wave should travel from the left to right in layer M2 via the turnover structure. Fig. 8 shows the traveling direction of the EM wave in layer M2, which is towards right direction.

D. WORKING MECHANISM
The rotation angles of the radiating and feeding parts are indicated as γ_d and γ_u, respectively, as shown in
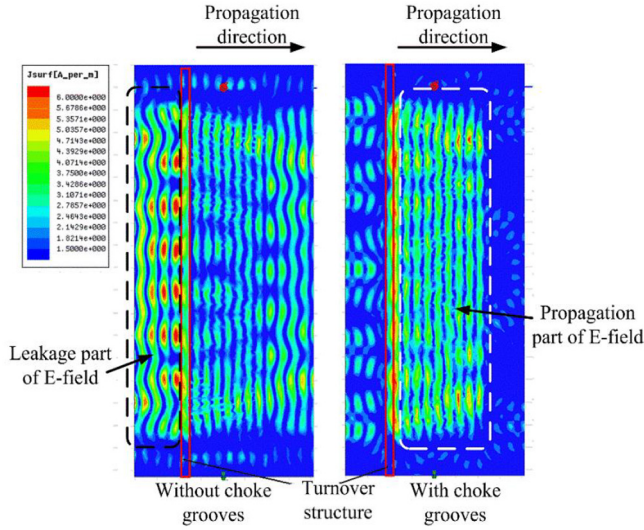
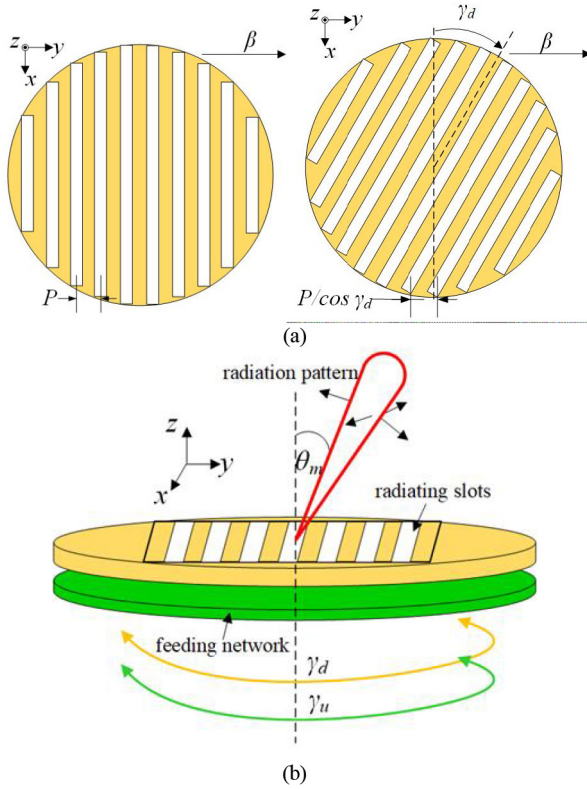**FIGURE 8.** E-field distribution of the antenna with and without high-impedance choke groove structure.

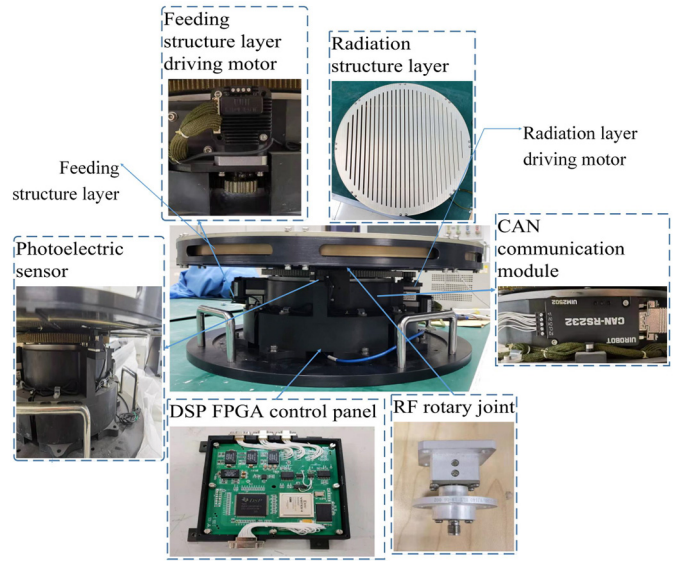**FIGURE 9.** Rotation of (a) the radiating part, and (b) the whole antenna.

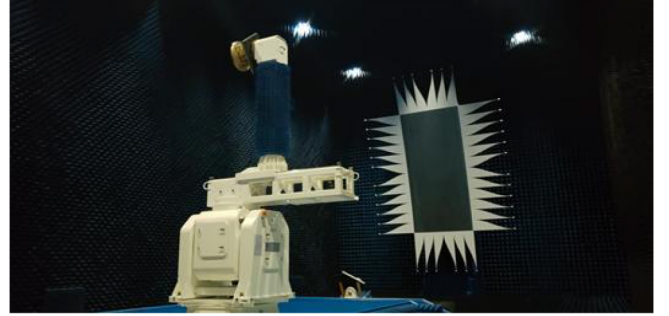**FIGURE 10.** The CTS array antenna system prototype.

FIGURE 11. Measurement of the proposed antenna in the anechoic chamber.

If $k_t^2 = k_0^2 - k_y^2 > 0$, the EM wave can be effectively radiated. To satisfy $k_t^2 = k_0^2 - k_y^2 > 0$, a substrate with permittivity of ε_r can be loaded between the radiating part and the PPW, or a slow-wave structure can be used to feed the slot array [21]. Thus, the period P should satisfy:

$$-\frac{2m\pi}{k_0(\sqrt{\varepsilon_r}+1)} < P < \frac{2m\pi}{k_0(1-\sqrt{\varepsilon_r})}, m = -1, -2, -3\ldots \quad (8)$$

By choosing the appropriate period P, a single radiation mode for $m = -1$ can be ensured.

When the rotation angle γ_u of the feeding parts keeps unchanged, but the radiating part has a rotation angle of γ_d, the period P becomes $P/\cos \gamma_d$. According to (7), for $m = -1$, the radiation angle of the main lobe is,

$$\theta = \sin^{-1}\left(\sqrt{\varepsilon_r} - \frac{\lambda}{P/\cos \gamma_d}\right) \quad (9)$$

Thus, beam scanning of the main lobe direction of θ_m can be realized by changing γ_d. When γ_d and γ_u have the same variation angle, i.e., $\Delta\gamma = 0$, the beam can be reconfigured within 360° in the azimuth angle. Thus, azimuth scanning

Fig. 9. When the relative rotation angle of the radiating and feeding parts is 0°, as depicted in Fig. 9(a), the y-component of the wavenumber k of the wave propagating of the radiating slots in the spherical coordinate is given by [27], [28]:

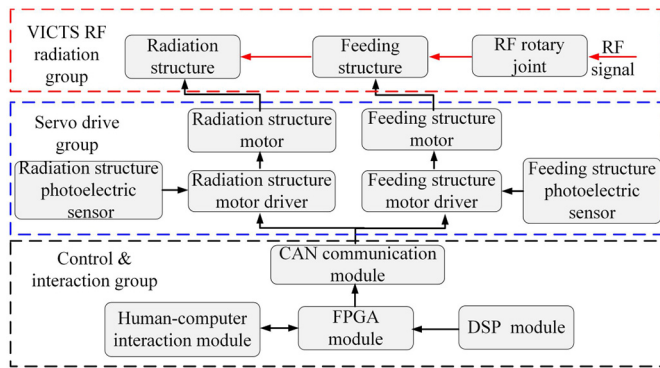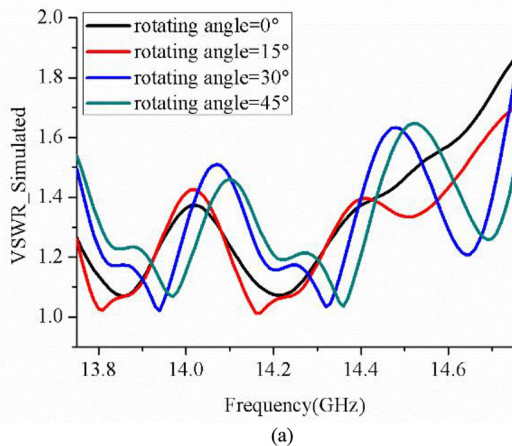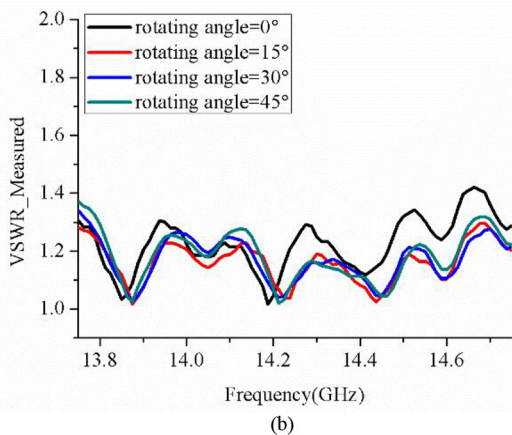$$k_y = k_0 \sin \theta_m = k_0\sqrt{\varepsilon_r} + 2m\pi/P, m = -1, -2, -3\ldots \quad (7)$$

FIGURE 12. The CTS array antenna system.

FIGURE 13. (a) Simulated and (b) measured reflection coefficients under different rotation angles.

FIGURE 14. Simulated radiation pattern at 14.25 GHz in the (a) E-plane, and (b) H-plane.

The antenna system prototype is shown in Fig. 10 and measured in the anechoic chamber in Fig. 11. In the practical model, two driving motors are used to rotate the feeding and radiating parts. The antenna system contains three parts, i.e., VICTS radiation antenna, servo drive group, and control and interaction part, as shown in Fig. 12. The VICTS RF radiation group includes RF rotary joint, feeding structure, and radiation structure. The feeding structure and the radiating structure are driven by the servo drive group. The radiating structure is directly controlled by the radiation structure motor activated by the motor driver. Similarly, the feeding structure is rotated by the feeding structure motor with the corresponding driver. Two photoelectric sensors are adopted to locate the initial zero position of the radiating and the feeding plates. The control and interaction group consists of a human-computer interaction module, a field-programmable gate array (FPGA) module, a Digital signal processing (DSP) module, and a Controller Area Network (CAN) communication module, supporting the motors of the radiation and the feeding structures. Through the CAN communication module, DSP and FPGA control panel is adopted to control the two motors according to the commands from the human-computer interaction module.

is attained when both radiating and feeding plates rotate synchronously, and elevation scanning is attained when they are rotated asynchronously.
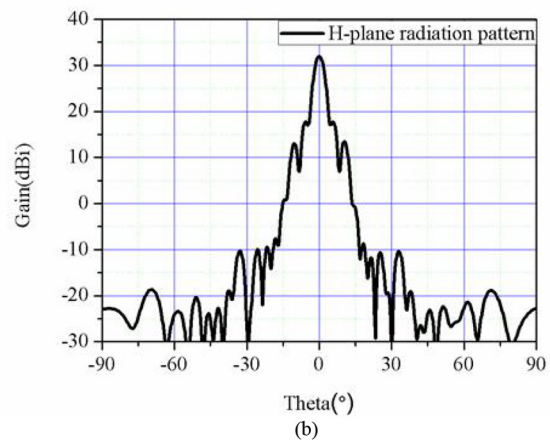
III. PROTOTYPE AND MEASURED RESULTS
A. VICTS ANTENNA SYSTEM
The VICTS antenna was first designed using the EM simulation tool HFSS, then fabricated and measured for verification.
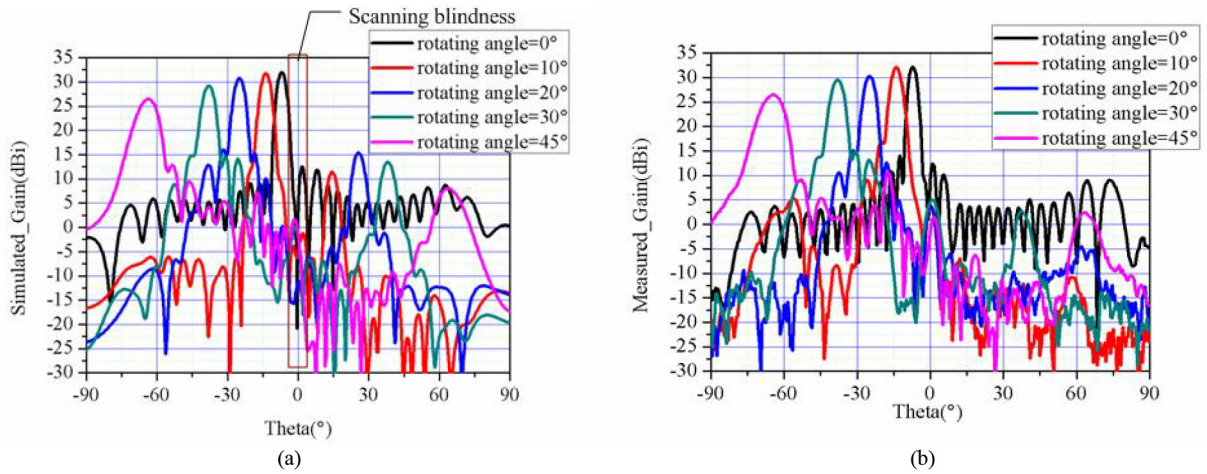
FIGURE 15. (a) Simulated, and (b) measured radiation patterns at 14.25 GHz under different rotation angles in the E-plane.
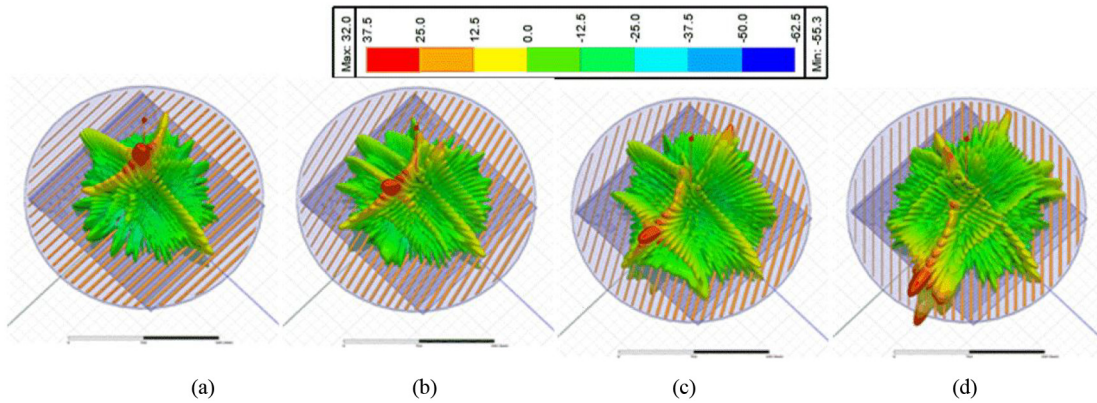

FIGURE 16. Simulated 3D radiation pattern at 14.25 GHz for the rotation angles of (a) 0°, (b) 15°, (c) 30°, and (d) 45°.

TABLE 2. Beam scanning angles at 14.25 GHz.

Rotation Angle /°	Beam Position /°				Gain /dBi		Beamwidth /°		Sidelobe	
	Sim.		Mea.		Sim.	Mea.	Sim.	Mea.	Sim.	Mea.
	Theta	Phi	Theta	Phi						
0	7.0	0	7.2	0	32.0	32.1	3.8	3.8	19.5	19.7
10	13.8	63	14.2	59.6	31.8	32.1	4.2	4.2	22.2	22.9
20	25.0	82	25.2	78	30.8	30.3	4.5	4.6	15.5	17.7
30	38.0	92	38	90.3	29.1	29.5	5.0	5.2	16.5	16.5
45	63.8	104	63.8	102.3	26.5	26.4	8.4	9	13.7	17.4

B. SIMULATED AND MEASURED RESULTS

When the rotation angle $\gamma_u = 0°$ of the feeding part remains unchanged, the simulated and measured reflection coefficients under different rotation angles γ_d of $0° - 45°$ are shown in Fig. 13. The remaining positions can be deduced by symmetry as the antenna structure is symmetrical. The simulated voltage standing wave ratio (VSWR) remains below 1.7 within 13.75–14.5 GHz when the rotating angle γ_d varies from $0°$ to $45°$, while the measured VSWR remains below 1.4 with different rotating angles. The result discrepancy is due to the fabrication and measurement tolerances.

When the rotation angle $\gamma_d = 0°$, the simulated radiation patterns at the center frequency of 14.25 GHz are shown in Fig. 14. The first sidelobe level (SLL) in H-plane is not obvious in Fig. 14(b), which can be neglected. It can be seen SLL in the E- and H-planes are about -19.5 dB, and a high gain of 32 dBi is obtained. The main beam of the proposed antenna has an angle of $7°$ deviating from the broadside direction in the E-plane. The low SLL is due to Taylor distribution of the radiation power for each slot based on the extracted admittances.

When the rotating angle γ_d varies from $0°$ to $45°$, the simulated and measured radiation patterns at 14.25 GHz in

TABLE 3. Comparison with other VICTS antenna.

Ref.	MSA	CF/ IMBW	Gain (dBi)	Aperture Efficiency	SLL (dB)
[5]	±40°	29.2/24%	28.9	39%	-11
[15]	±30°	15.5/3.2%	30.7	-	-15.4
[17]	±40°	29/17.2%	28	24.6%	-12.8
[18]	±58°	61.5/13%	29.3	61%	-15
[23]	±60°	29.2/2.7%	28.5	55%	-9
Pro.	±64°	14.25/5.3%	32.1	51.4%	-16.5

MSA: maximum scanning angle, CF: center frequency.

the H-plane are shown in Fig. 15. It can be seen a large beam scanning range is achieved, with the elevation angle θ changing from $-7°$ to $-64°$. Due to the symmetric structure, $7°$ to $64°$ beam scanning can also be realized. In azimuth, a $360°$ scanning range can be achieved by rotating the radiating and feeding parts together. The simulated patterns superimpose with the measured patterns, and the measured SLL remains lower than -16.5 dB for all the rotation angles.

For clearly seeing the beam scanning performance, the simulated 3D radiation patterns at 14.25 GHz for the rotation angles of $0°$ to $45°$ with a step of $15°$ are shown in Fig. 16. It can be found the main beam exhibits a large scanning range. The detailed radiation information is given in Table 2, indicating that the simulated and measured results match well. The biggest gain drop for all the scanning radiation patterns is 5.5 dB and 5.7 dB for simulated and measured results, respectively. According to,

$$G = \eta \frac{4\pi A}{\lambda^2} \tag{10}$$

where G is gain, A is effective area, λ is the wavelength of the working frequency, and η is the aperture efficiency. The aperture radiation efficiency of the proposed antenna for the central beam is about 51.4%.

Finally, the performance of the proposed VICTS antenna is compared with other works in Table 3. The maximum scanning angle in elevation reaches up to 64°, within which the sidelobes of the radiation patterns are less than -16.5 dB, smaller than other works. Meanwhile, the peak gain and the aperture efficiency are relatively high.

IV. CONCLUSION

A beam-scanning antenna system for SatCom on the move is proposed. This antenna system consists of a VICTS radiation antenna, a servo driver group, and a control and interaction part. Large beam scanning range, continuous beam steering, high gain, and low SLL performances can be realized. Moreover, the servo control system is combined with the VICTS antenna to make it more attractive for vehicle-to-satellite communication terminals with moving platforms.

REFERENCES

[1] R. A. Pearson, J. Vazquez, M. W. Shelley, A. Payne, V. Stoiljkovic, and M. Steel, "Next generation mobile SATCOM terminal antennas for a transformed world," in *Proc. IEEE 5th Eur. Conf. Antennas Propag. (EUCAP)*, Rome, Italy, 2011, pp. 2341–2345.

[2] G. L. He, X. Gao, L. L. Sun, and R. T. Zhang, "A review of multibeam phased array antennas as LEO satellite constellation ground station," *IEEE Access*, vol. 9, pp. 147142–147154, 2021.

[3] J. L. G. Tornero, A. Martínez, M. P. García, and D. C. Rebenaque, "ARIEL: Passive beam-scanning antenna terminal for iridescent and efficient LEO satellite connectivity," *IEEE Antennas Wireless Propag. Lett.*, early access, Jul. 22, 2022, doi: 10.1109/LAWP.2022.3193040.

[4] N. Rezazadeh and L. Shafai, "Ultrawideband monopulse antenna with application as a reflector feed," *IET Microw. Antennas Propag.*, vol. 10, no. 4, pp. 393–400, 2016.

[5] M. Ettorre, F. F. Manzillo, M. Casaletti, R. Sauleau, L. L. Coq, and N. Capet, "Continuous transverse stub array for Ka-band applications," *IEEE Trans. Antennas Propag.*, vol. 63, no. 6, pp. 4792–4800, Nov. 2015.

[6] V. F. Fusco, "Mechanical beam scanning reflectarray," *IEEE Trans. Antennas Propag.*, vol. 53, no. 11, pp. 3842–3844, Nov. 2005.

[7] H. L. Zhu, S. W. Cheung, and T. I. Yuk, "Mechanically pattern reconfigurable antenna using metasurface," *IET Microw. Antennas Propag.*, vol. 9, pp. 1331–1336, Sep. 2015.

[8] H. Bolandhemmat, M. Fakharzadeh, P. Mousavi, S. H. Jamali, G. Z. Rafi, and S. Safavi-Naeini, "Active stabilization of vehicle-mounted phased-array antennas," *IEEE Trans. Veh. Technol.*, vol. 58, no. 6, pp. 2638–2650, Jul. 2009.

[9] G. Jin, M. Li, D. Liu, and G. Zeng, "A simple planar pattern-reconfigurable antenna based on arc dipoles," *IEEE Antennas Wireless Propag. Lett.*, vol. 17, pp. 1664–1668, 2018.

[10] J.-S. Row and L.-K. Kuo, "Pattern-reconfigurable array based on a circularly polarized antenna with broadband operation and high front-to-back ratio," *IEEE Trans. Antennas Propag.*, vol. 68, no. 5, pp. 4109–4113, May 2020.

[11] W. Lin, H. Wong, and R. W. Ziolkowski, "Wideband pattern-reconfigurable antenna with switchable broadside and conical beams," *IEEE Antennas Wireless Propag. Lett.*, vol. 16, pp. 2638–2641, 2017.

[12] P.-Y. Qin, Y. J. Guo, and C. Ding, "A beam switching quasi-yagi dipole antenna," *IEEE Trans. Antennas Propag.*, vol. 61, no. 10, pp. 4891–4899, Oct. 2013.

[13] W. W. Milroy, "Antenna array configurations employing continuous transverse stub elements," U.S. Patent 5 349 363, 1994.

[14] W. H. Henderson and W. W. Milroy, "Wireless communication applications of the continuous transverse stub (CTS) array at microwave and millimeter wave frequencies," in *Proc. IEEE/ACES Int. Conf. Wireless Commun. Appl. Comput. Electromagn.*, Honolulu, HI, USA, 2005, pp. 253–256.

[15] X. Lu, S. Gu, X. Wang, H. Liu, and W. Lu, "Beam-scanning continuous transverse stub antenna fed by a ridged waveguide slot array," *IEEE Antennas Wireless Propag. Lett.*, vol. 16, pp. 1675–1678, 2017.

[16] F. F. Manzillo et al., "A multilayer LTCC solution for integrating 5G access point antenna modules," *IEEE Trans. Microw. Theory Techn.*, vol. 64, no. 7, pp. 2272–2283, Jul. 2016.

[17] W. P. Wang, Q. L. Huang, Z. X. Liu, H. Liu, and X. W. Shi, "A beam scanning continuous transverse stub array antenna for Ka-band applications," *Microw. Opt. Technol. Lett.*, vol. 61, no. 4, pp. 1097–1103, Apr. 2019.

[18] K. Tekkouk, J. Hirokawa, R. Sauleau, and M. Ando, "Wideband and large coverage continuous beam steering antenna in the 60-GHz band," *IEEE Trans. Antennas Propag.*, vol. 65, no. 9, pp. 4418–4426, Sep. 2017.

[19] Y. You, Y. Lu, Q. You, Y. Wang, J. Huang, and M. J. Lancaster, "Millimeter-wave high-gain frequency-scanned antenna based on waveguide continuous transverse stubs," *IEEE Trans. Antennas Propag.*, vol. 66, no. 11, pp. 6370–6375, Nov. 2018.

[20] Y. Li, M. F. Iskander, Z. Zhang, and Z. Feng, "A new low cost leaky wave coplanar waveguide continuous transverse stub antenna array using metamaterial-based phase shifters for beam steering," *IEEE Trans. Antennas Propag.*, vol. 61, no. 7, pp. 3511–3518, Jul. 2013.

[21] M. F. Iskander, Z. Yun, Z. Zhang, R. Jensen, and S. Redd, "Design of a low-cost 2-D beam-steering antenna using ferroelectric material and CTS technology," *IEEE Trans. Microw. Theory Techn.*, vol. 49, no. 5, pp. 1000–1003, May 2001.

[22] R. Isom, M. F. Iskander, Z. Yun, and Z. Zhang, "Design and development of multiband coaxial continuous transverse stub (CTS) antenna arrays," *IEEE Trans. Antennas Propag.*, vol. 52, no. 8, pp. 2180–2184, Aug. 2004.

[23] R. S. Hao, Y. J. Cheng, and Y. F. Wu, "Shared-aperture variable inclination continuous transverse stub antenna working at K- and Ka-bands for mobile satellite communication," *IEEE Trans. Antennas Propag.*, vol. 68, no. 9, pp. 6656–6666, Sep. 2020.

[24] Y.-L. Lyu et al., "Leaky-wave antennas based on noncutoff substrate integrated waveguide supporting beam scanning from backward to forward," *IEEE Trans. Antennas Propag.*, vol. 64, no. 6, pp. 2155–2164, Jun. 2016.

[25] R. Elliott, "On the design of traveling-wave-fed longitudinal shunt slot arrays," *IEEE Trans. Antennas Propag.*, vol. AP-27, no. 5, pp. 717–720, Sep. 1979.

[26] H. M. El Misilmani, M. Al-Husseini, and K. Y. Kabalan, "Design of slotted waveguide antennas with low sidelobes for high power microwave applications," *Progr. Electromagn. Res. C*, vol. 56, pp. 15–28, Jan. 2015.

[27] J. H. Wang and K. K. Mei, "Theory and analysis of leaky coaxial cables with periodic slots," *IEEE Trans. Antennas Propag.*, vol. 49, no. 12, pp. 1723–1732, Dec. 2001.

[28] A. K. Bhattacharyya, "Theory of beam scanning for slot array antenna excited by slow wave," *IEEE Antennas Propag. Mag.*, vol. 57, no. 2, pp. 96–103, Apr. 2015.